Prototype of an ultra-stable optic cavity for space applications

Bérengère Argence, Eddie Prevost, Thomas Lévèque, Roland Le Goff, Pierre Lemonde, Sebastien Bize, Giorgio Santarelli

Prototype of an ultra-stable optical cavity for space applications.

B. Argence,[1,*] E. Prevost,[2] T. Lévèque,[3] R. Le Goff,[2] S. Bize,[1] P. Lemonde,[1] and G. Santarelli[1,4]

[1] *Laboratoire national de métrologie et d'essais - Systèmes de Références Temps-Espace, Observatoire de Paris, CNRS, UMR 8630, 61 Av. de l'Observatoire, 75014 Paris, France*
[2] *SODERN, 20 Av. Descartes, 94451 Limeil-Brevannes, France*
[3] *Centre National d'Etudes Spatiales, 18 Av. Edouard Belin, 31401 Toulouse, France*
[4] *Laboratoire Photonique, Numérique et Nanosciences, Université de Bordeaux, Institut d'Optique Graduate School, CNRS, UMR 5298, 351 cours de la Libération, 33405 Talence, France*
[*] *berengere.argence@obspm.fr*

Abstract: We report the main features and performances of a prototype of an ultra-stable cavity designed and realized by industry for space applications with the aim of space missions. The cavity is a 100 mm long cylinder rigidly held at its midplane by a engineered mechanical interface providing an efficient decoupling from thermal and vibration perturbations. Intensive finite element modeling was performed in order to optimize thermal and vibration sensitivities while getting a high fundamental resonance frequency. The system was designed to be transportable, acceleration tolerant (up to several g) and temperature range compliant $[-33^{\circ}\mathrm{C}\ ;\ 73^{\circ}\mathrm{C}]$. Thermal isolation is ensured by gold coated Aluminum shields inside a stainless steel enclosure for vacuum. The axial vibration sensitivity was evaluated at $(4 \pm 0.5) \times 10^{-11}/(\mathrm{m.s}^{-2})$, while the transverse one is $< 1 \times 10^{-11}/(\mathrm{m.s}^{-2})$. The fractional frequency instability is $\lesssim 1 \times 10^{-15}$ from 0.1 to a few seconds and reaches $5-6 \times 10^{-16}$ at 1s.

OCIS codes: (120.3930) Metrological instrumentation; (120.6085) Space instrumentation; (120.2230) Fabry-Perot; (140.3425) Laser stabilization; (140.4780) Optical resonators.

References and links

1. H. Katori, "Optical lattice clocks and quantum metrology," Nature Photon. **5**, 203–210 (2011).
2. M. D. Swallows, M. Bishof, Y. Lin, S. Blatt, M. J. Martin, A. M. Rey, and J. Ye, "Suppression of collisional shifts in a strongly interacting lattice clock," Science **331**, 1043–1046 (2011).
3. N. Huntemann, M. Okhapkin, B. Lipphardt, S. Weyers, C. Tamm, and E. Peik, "High-accuracy optical clock based on the octupole transition in $^{171}Yb^{+}$," Phys. Rev. Lett. **108**, 090801 (2012).
4. J. Sherman, N. Lemke, N. Hinkley, M. Pizzocaro, R. Fox, A. Ludlow, and C. Oates, "High-accuracy measurement of atomic polarizability in an optical lattice clock," Phys. Rev. Lett. **108**, 153002 (2012).
5. J. J. McFerran, L. Yi, S. Mejri, S. Di Manno, W. Zhang, J. Guéna, Y. Le Coq, and S. Bize, "Neutral atom frequency reference in the deep ultraviolet with fractional uncertainty = 5.7×10^{-15}," Phys. Rev. Lett. **108**, 183004 (2012).
6. F. Acernese, M. Alshourbagy, P. Amico, F. Antonucci, S. Aoudia, K. G. Arun, P. Astone, S. Avino, L. Baggio, G. Ballardin, F. Barone, L. Barsotti, M. Barsuglia, T. S. Bauer, S. Bigotta, S. Birindelli, M. A. Bizouard, C. Boccara, F. Bondu, L. Bosi, S. Braccini, C. Bradaschia, A. Brillet, V. Brisson, D. Buskulic, G. Cagnoli, E. Calloni, E. Campagna, F. Carbognani, F. Cavalier, R. Cavalieri, G. Cella, E. Cesarini, E. Chassande-Mottin, S. Chatterji, F. Cleva, E. Coccia, C. Corda, A. Corsi, F. Cottone, J.-P. Coulon, E. Cuoco, S. D'Antonio, A. Dari, V. Dattilo, M. Davier, R. D. Rosa, M. D. Prete, L. D. Fiore, A. D. Lieto, M. D. P. Emilio, A. D. Virgilio, M. Evans,

#172506 - $15.00 USD Received 12 Jul 2012; accepted 5 Oct 2012; published 25 Oct 2012

V. Fafone, I. Ferrante, F. Fidecaro, I. Fiori, R. Flaminio, J.-D. Fournier, S. Frasca, F. Frasconi, L. Gammaitoni, F. Garufi, E. Genin, A. Gennai, A. Giazotto, V. Granata, C. Greverie, D. Grosjean, G. Guidi, S. Hamdani, S. Hebri, H. Heitmann, P. Hello, D. Huet, P. L. Penna, M. Laval, N. Leroy, N. Letendre, B. Lopez, M. Lorenzini, V. Loriette, G. Losurdo, J.-M. Mackowski, E. Majorana, N. Man, M. Mantovani, F. Marchesoni, F. Marion, J. Marque, F. Martelli, A. Masserot, F. Menzinger, L. Milano, Y. Minenkov, M. Mohan, J. Moreau, N. Morgado, S. Mosca, B. Mours, I. Neri, F. Nocera, G. Pagliaroli, C. Palomba, F. Paoletti, S. Pardi, A. Pasqualetti, R. Passaquieti, D. Passuello, F. Piergiovanni, L. Pinard, R. Poggiani, M. Punturo, P. Puppo, O. Rabaste, P. Rapagnani, T. Regimbau, A. Remillieux, F. Ricci, I. Ricciardi, A. Rocchi, L. Rolland, R. Romano, P. Ruggi, D. Sentenac, S. Solimeno, B. L. Swinkels, R. Terenzi, A. Toncelli, M. Tonelli, E. Tournefier, F. Travasso, G. Vajente, J. F. J. van den Brand, S. van der Putten, D. Verkindt, F. Vetrano, A. Vicer?, J.-Y. Vinet, H. Vocca, and M. Yvert, "Virgo status," Class. Quantum Grav. **25**, 184001 (2008).

7. S. Herrmann, A. Senger, K. Mohle, M. Nagel, E. Kovalchuk, and A. Peters, "Rotating optical cavity experiment testing Lorentz invariance at the 10^{-17} level," Phys. Rev. D **80**, 105011 (2009).
8. C. W. Chou, D. B. Hume, T. Rosenband, and D. J. Wineland, "Optical clocks and relativity," Science **329**, 1630–1633 (2010).
9. H. Jiang, F. Kéfélian, S. Crane, O. Lopez, M. Lours, J. Millo, D. Holleville, P. Lemonde, C. Chardonnet, A. Amy-Klein, and G. Santarelli, "Long-distance frequency transfer over an urban fiber link using optical phase stabilization," J. Opt. Soc. Am. B. **25**, 2029–2035 (2008).
10. K. Predehl, G. Grosche, S. M. F. Raupach, S. Droste, O. Terra, J. Alnis, T. Legero, T. W. H?nsch, T. Udem, R. Holzwarth, and H. Schnatz, "A 920-kilometer optical fiber link for frequency metrology at the 19th decimal place," Science **336**, 441–444 (2012).
11. K. Danzmann and A. Rüdiger, "Lisa technology - concept, status, prospects," Class. Quantum Grav. **20**, S1 (2003).
12. K. Numata, A. Kemery, and J. Camp, "Thermal-noise limit in the frequency stabilization of lasers with rigid cavities," Phys. Rev. Lett. **93**, 250602 (2004).
13. T. Legero, T. Kessler, and U. Sterr, "Tuning the thermal expansion properties of optical reference cavities with fused silica mirrors," J. Opt. Soc. Am. B. **27**, 914–919 (2010).
14. T. Kessler, T. Legero, and U. Sterr, "Thermal noise in optical cavities revisited," J. Opt. Soc. Am. B **29**, 178–184 (2012).
15. T. Kessler, C. Hagemann, C. Grebing, T. Legero, U. Sterr, F. Riehle, M. J. Martin, L. Chen, and J. Ye, "A sub-40 mHz linewidth laser based on a silicon single-crystal optical cavity," Nature Photon. **6**, 687–692 (2012).
16. A. D. Ludlow, X. Huang, M. Notcutt, T. Zanon-Willette, S. M. Foreman, M. M. Boyd, S. Blatt, and J. Ye, "Compact, thermal-noise-limited optical cavity for diode laser stabilization at 1×10^{-15}," Opt. Lett. **32**, 641–643 (2007).
17. S. A. Webster, M. Oxborrow, S. Pugla, J. Millo, and P. Gill, "Thermal-noise-limited optical cavity," Phys. Rev. A **77**, 033847 (2008).
18. Y. Y. Jiang, A. D. Ludlow, N. D. Lemke, R. W. Fox, J. A. Sherman, L.-S. Ma, and C. W. Oates, "Making optical atomic clocks more stable with 10^{-16}−level laser stabilization," Nature Photon. **5**, 158–161 (2011).
19. J. Millo, D. V. Magalhães, C. Mandache, Y. Le Coq, E. M. L. English, P. G. Westergaard, J. Lodewyck, S. Bize, P. Lemonde, and G. Santarelli, "Ultrastable lasers based on vibration insensitive cavities," Phys. Rev. A **79**, 053829 (2009).
20. S. Webster and P. Gill, "Force-insensitive optical cavity," Opt. Lett. **36**, 3572–3574 (2011).
21. S. Vogt, C. Lisdat, T. Legero, U. Sterr, I. Ernsting, A. Nevsky, and S. Schiller, "Demonstration of a transportable 1 Hz-linewidth laser," Appl. Phys. B **104**, 741–745 (2011).
22. D. R. Leibrandt, M. J. Thorpe, J. C. Bergquist, and T. Rosenband, "Field-test of a robust, portable, frequency-stable laser," Opt. Express **19**, 10278–10286 (2011).
23. P. Laurent, M. Abgrall, C. Jentsch, P. Lemonde, G. Santarelli, A. Clairon, I. Maksimovic, S. Bize, C. Salomon, D. Blonde, J. Vega, O. Grosjean, F. Picard, M. Saccoccio, M. Chaubet, N. Ladiette, L. Guillet, I. Zenone, C. Delaroche, and C. Sirmain, "Design of the cold atom PHARAO space clock and initial test results," Appl. Phys. B **84**, 683–690 (2006).
24. R. W. P. Drever, J. L. Hall, F. V. Kowalski, J. Hough, G. M. Ford, A. J. Munley, and H. Ward, "Laser phase and frequency stabilization using an optical resonator," Appl. Phys. B **31**, 97–105 (1983).
25. The USL is a high-finesse FP cavity stabilized laser at 1.54μm described in [9]. The fractional frequency stability is 1×10^{-15} at 1s dominated by the thermal noise limit (all-ULE cavity).
26. S. Dawkins, R. Chicireanu, M. Petersen, J. Millo, D. Magalhaes, C. Mandache, Y. Le Coq, and S. Bize, "An ultra-stable referenced interrogation system in the deep ultraviolet for a mercury optical lattice clock," Appl. Phys. B **99**, 41–46 (2010).
27. J. J. McFerran, D. V. Magalhaes, C. Mandache, J. Millo, W. Zhang, Y. Le Coq, G. Santarelli, and S. Bize, "Laser locking to the ^{199}Hg $^1S_0$-$^3P_0$ clock transition with $5.4\times10^{-15}/\sqrt{\tau}$ fractional frequency instability," Opt. Lett. **37**, 3477–3479 (2012).

#172506 - $15.00 USD Received 12 Jul 2012; accepted 5 Oct 2012; published 25 Oct 2012

1. Introduction

Ultra-stable lasers are key elements in modern physics covering a wide range of applications in frequency metrology [1–5], gravitational wave detection [6], fundamental physics tests [7, 8], coherent optical links [9, 10] and related space applications [11]. Frequency stability can be achieved by locking the laser onto a rigid Fabry-Perot (FP) cavity, the stability of the laser is then defined by the stability of the optical length of the reference cavity. The ultimate fundamental limit of this system is the thermal noise (Brownian motion) that can be minimized by optimizing the choice of the cavity materials and geometry [12–14] and reducing the cavity temperature with cryogenic techniques [15]. Nevertheless, to reach this limit, different sources of noise have to be drastically reduced. Among them, the most important ones are thermal and vibration perturbations. During the last decade, much effort has been devoted to isolating cavities and making them insensitive by design to environmental perturbations. The thermal noise limit has been reached by different groups [16, 17] down to a few 10^{-16} fractional frequency stability [18, 19].

A number of applications require an ultra-stable laser available for use in a non-laboratory environment [8, 11]. Nonetheless, most of these cavities have been designed with a laboratory in view and making them compatible with transport and space requirements involves a major redesign of the cavity and its assembly. One of the most sensitive point is that these cavities are usually not rigidly held but only supported under their own weight which is obviously not compatible with robustness or transport requirements. Rigidly attaching the cavity creates mechanical constraints on its structure that will potentially increase its vibration sensitivity. A new approach is then necessary. Recently, in this aim, significant progress towards cavity designs with low vibration sensitivity [20], transportability [21] and robustness [22] has been achieved.

This work reports on the design and realization of an ultra-stable cavity by space industry. The main objective of this study is the development of key technologies for future reference optical cavities in space to reach a TRL (Technical Readiness Level) of 5. It is worth recalling that the methods used during the conception of this prototype are compliant with space engineering and have clear synergies with the PHARAO space clock development [23]. Nevertheless, the advanced technologies used for the PHARAO flight model that can be transferred seamlessly on this equipment are not used on this first design due to cost constraint and schedule. The main idea is then to capitalize on the space instrument development know-how to accommodate for constraints not usual in a laboratory environment. The device is designed to be able to resist acceleration up to 20(6)g along the axial (transverse) axis and temperature variations in the range of $[-33^{\circ}\mathrm{C}\ ;\ 73^{\circ}\mathrm{C}]$ during transport and storage, while keeping good frequency stability performances in operation conditions. Extensive thermo-mechanical modeling was thus performed in order to obtain low thermal and vibration sensitivities. In this paper, we will first focus the cavity design and the Finite Element Modeling (FEM) that have been carried out (section 2). The experimental setup to frequency lock a laser on the cavity resonance is then detailed in section 3. Section 4 presents the thermal and vibration characterization of the cavity assembly. The fractional frequency stability and the frequency noise spectral density results are given in section 5. Section 6 summarizes the main points developed in the paper and provides prospects for future versions.

2. Finite element modeling

The cavity assembly is a cylindrical optical reference cavity rigidly held at its midplane by a mechanical interface and isolated from thermal perturbations by two aluminum shield and a vacuum enclosure. In this section, we will first present the cavity design and geometry and introduce some crucial parameters of the finite element simulation. In a second part, the me-

#172506 - $15.00 USD Received 12 Jul 2012; accepted 5 Oct 2012; published 25 Oct 2012

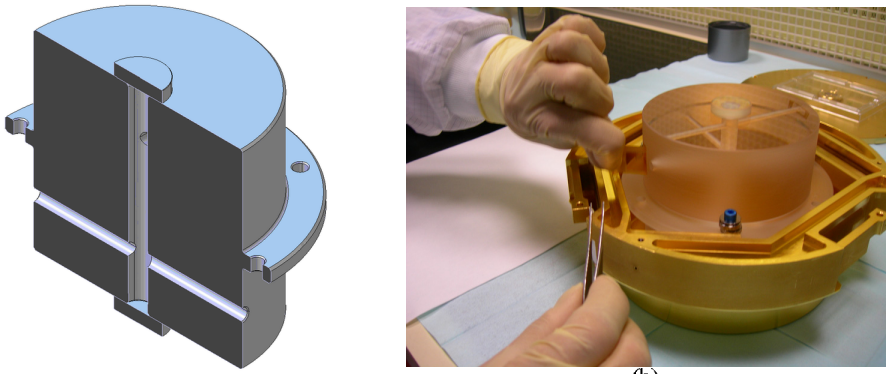

(a) (b)

Fig. 1. (a) Cross section drawing of the cavity showing the cavity spacer and the mirrors, the central ring with fixation holes, and the two through venting holes. (b) Photography of the cavity mounted on the Cavity Fastening Device, see text for details.

chanical interface allowing rigid attachment of the cavity to the inner shield will be detailed and the last part is dedicated to the thermal isolation.

2.1. Cavity design and geometry

The cavity has a cylindrical geometry of length 100 mm and diameter 110 mm (see Fig. 1). The reflection coating of the mirrors allows operation at 1.542μm, in the telecom wavelength region. The free spectral range is 1.5 GHz. The mirror configuration is plano-concave (radius of curvature of 500mm). The spacer is made of Ultra-Low Expansion (ULE) glass, with Fused Silica (FS) mirrors substrates in order to reduce the thermal noise floor. For the present geometry, the estimated flicker thermal noise is $\sim 4\times10^{-16}$, dominated by the mechanical quality factor of the coatings [12, 14, 19]. This is a factor >2 better than an all-ULE cavity. The main drawback of this approach is an increase of the Coefficient of Thermal Expansion (CTE) to about $\sim 10^{-7}$/K, a value that we verified experimentally, due to the mismatch between the CTE of the FS substrate and that of the ULE (FS CTE $\sim 5\times10^{-7}$/K, ULE CTE $< 10^{-8}$/K)). Consequently, the effective CTE of the cavity is higher than that of an all-ULE cavity. To overcome this problem in a next generation of cavities, we could implement the technique proposed by Legero et al. [13], which consists in compensating the high FS CTE by optical contacting a specially engineered ULE ring on the mirror substrate. An improvement of at least one order of magnitude can be expected without any degradation of the thermal noise limit [14].

A ring in the midplane of the cylinder allows rigid attachment of the cavity (see Fig. 1). The cavity body is machined from a monolithic block of ULE. The ring has a diameter of 140mm and a thickness of 7mm. Six holes distributed equidistantly were drilled, corresponding to two sets of three holes possible to fix the cavity. The cavity is then held symmetrically at three points (at 120 degrees) by a mechanical interface called the Cavity Fastening Device (CFD), described in paragraph 2.2. The shape of the central ring (thickness and diameter) is the result of a complex trade-off between volume, vibration sensitivity, fastening interface dimensions and machining constrains. The diameter of the spacer was optimized to minimize the transverse vibration sensitivities. This approach was already successfully applied in the vertical cavity of Ref. [19]. Additional simulations were performed to evaluate the CFD impact. The trade-off between dimensions and performances appears for a diameter of 110mm. The position of the venting holes (VH), see Fig. 1(a), was determined so as to maintain stiffness and to minimize

#172506 - $15.00 USD Received 12 Jul 2012; accepted 5 Oct 2012; published 25 Oct 2012

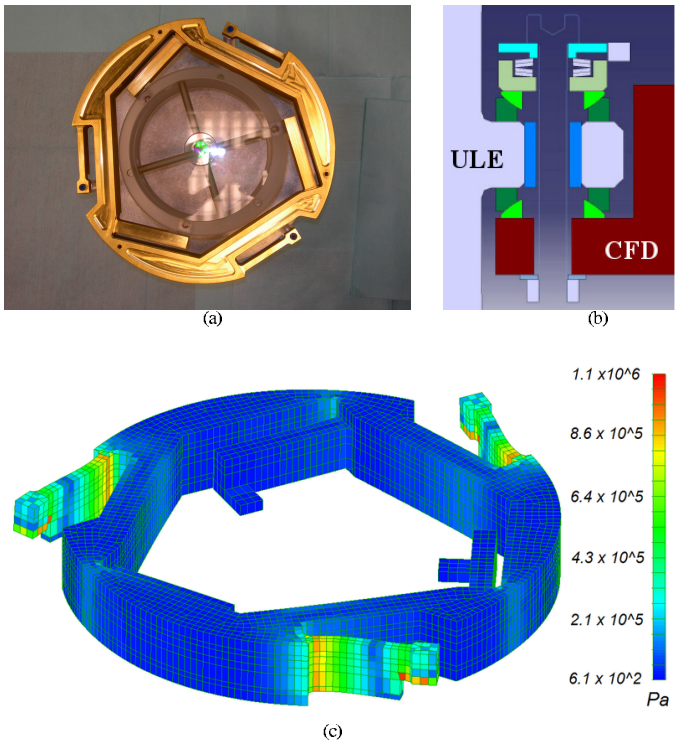

Fig. 2. (a) Photography of the cavity and its Cavity Fastening Device (CFD), see text for details. (b) Drawing of the cavity to the CFD interface assembly. (c) Finite Element Method of the CFD under 1°C of temperature change (Von Mises stress).

the asymmetry of the spacer. Three different configurations have been studied. In each case, the axes of the VH were in two parallel planes, equidistant from the ring. In the first configuration, the axes are perpendicular to each other. In the two others, they are parallel, but present different orientations relative to the attachment points to the CFD. The chosen configuration is the first one, which shows the results closest to that without holes (minimization of the horizontal vibration sensitivity). In-depth FEM analyses were performed on the cavity itself to take into account machining or assembly tolerances. For example, a vertical offset of 1 mm of the ring position leads to a degradation of the vertical vibration sensitivity of $1 \times 10^{-11}/(\mathrm{m.s}^{-2})$. A shift of 1 degree of one of the three attaching points implies an increase of the transverse vibration sensitivity to $5 \times 10^{-12}/(\mathrm{m.s}^{-2})$, while an angular shift between the plane of the mirrors and the plane of the CFD generates a small degradation of $5 \times 10^{-13}/(\mathrm{m.s}^{-2})$/degree on the vertical sensitivity. The effect of the cavity machining tolerances on the vibration sensitivity has then been carefully evaluated, leading to a set of constraints to minimize their impact.

2.2. Mechanical interface - Cavity Fastening Device (CFD)

A critical part of the system is the interface between the cavity and the inner thermal shield. The interface is designed to decouple both mechanically and thermally the cavity. In addition, the interface needs to preserve the properties of the cavity design in terms of mechanical symmetry. The overall task is complicated by the significant mass of the cavity of about 2.2kg. Considerable efforts have been devoted to model the CFD, as depicted in Fig. 2. This interface is machined from Invar, in order to reduce the differential temperature expansions between the

#172506 - $15.00 USD Received 12 Jul 2012; accepted 5 Oct 2012; published 25 Oct 2012

cavity spacer and the CFD and consequently to minimize stresses and deformations applied to the cavity. A dual cantilever system rigidly links the central ring of the CFD to the cavity and the inner thermal shield. The cantilever beams are designed to attenuate stress and deformation due to temperature variations and assembly defaults while maintaining a high degree of stiffness and consequently a sufficiently high fundamental Eigen mode. For instance, the section of the outer beams allows absorbing the large differential expansion between the CFD central ring and the thermal shield (3×10^{-5}/K). Figure 2(c) gives a representation of the Von Mises stress of the CFD when a 1°C temperature change is applied. The maximum stress observed on the CFD is $\sim$ 1MPa/°C. Even for 50°C temperature variation the maximum stress is well below the Invar yield stress point ($\sim$ 300MPa). The inner beams section is larger to increase stiffness and thus transmits negligible deformations to the cavity. Moreover, as for the outer cantilevers, their geometry is optimized to compensate the CTE gap between the CFD and the ULE. In addition the Invar low temperature coefficient leads to a modest $\sim$ 1.5MPa stress for a temperature variation of 50°C, far from the ULE ultimate tensile strength ($\sim$ 50MPa). The first mechanical resonance of the whole system - excluding the holding posts - was designed to be $\sim$ 300Hz, quite high considering the mass of the system (40 kg). To avoid torque and to prevent ULE glass damage/breakage, the interface between the glass and the inner cantilevers was specifically studied and optimized. The cavity and the CFD are bolted together with an optimized stack of washers, see Fig. 2(b). The use of elastic washers and an optimized assembly procedure allow applying a calibrated tensile load with null torque and local deformations below a few microns. The initial calibration of these washers before integration enables one to control the clamping force during the integration process. The value of the preload is directly linked to the maximal acceleration that the mounting can withstand. The minimum guarantee preload applied on each screwed link is about $\sim$ 420N, with such a preload, the assembly can withstand $\sim$ 6g of quasi static transverse acceleration without sliding. The admissible value is computed by applying space application dimensioning rules and taking into account a minimum safety coefficient of 30%. The value of $\sim$ 6g is potentially compliant with space application if the cavity assembly is mounted on dampers, filtering the launch vibrations and the pyrotechnic shocks. Moreover, for this study, we assume the tensile yield stress in ULE as the dimensioning parameter. It is a conservative approach since the compressive yield stress is much higher. Several tests have then been done showing that ULE can withstand a much higher preload up to $\sim$ 2600N. With such a value, the assembly will be compliant with $\sim$ 37g of quasi static acceleration. The maximum admissible axial acceleration is not limited by sliding effects and its value is higher than $\sim$ 20g. These already good results can be significantly improved if one reduces the length and thus the mass of the cavity.

2.3. Thermal shields

An efficient thermal isolation strategy is mandatory to ensure frequency stability performances. The cavity is protected against thermal perturbations by two gold coated aluminum shields inside a stainless steel vacuum chamber, as presented in Fig. 3. A third thin thermal heat shield is inserted between the cavity and the inner shield and directly fixed on the CFD, see Fig 3(a). Both the stainless steel enclosure and the thermal shields are polished to reduce their emissivities. To keep the first mechanical resonance as high as possible and to be compatible with the requirements of transport, each shield is rigidly fixed to the outer one. Mechanical standoffs in titanium are used to minimize the thermal conductance between the shields. Their position is also optimized by thermal modeling to increase the thermal path. Two sets of three standoffs on two parallel planes are used to connect each shield to the outer one. Then, from one shield to the other, a 60 degrees rotation of the sets around the vertical axis is applied. This passive thermal shielding behaves as a second order low pass filter with time constants close to $\sim$ 0.9 and $\sim$ 2.5

#172506 - $15.00 USD Received 12 Jul 2012; accepted 5 Oct 2012; published 25 Oct 2012

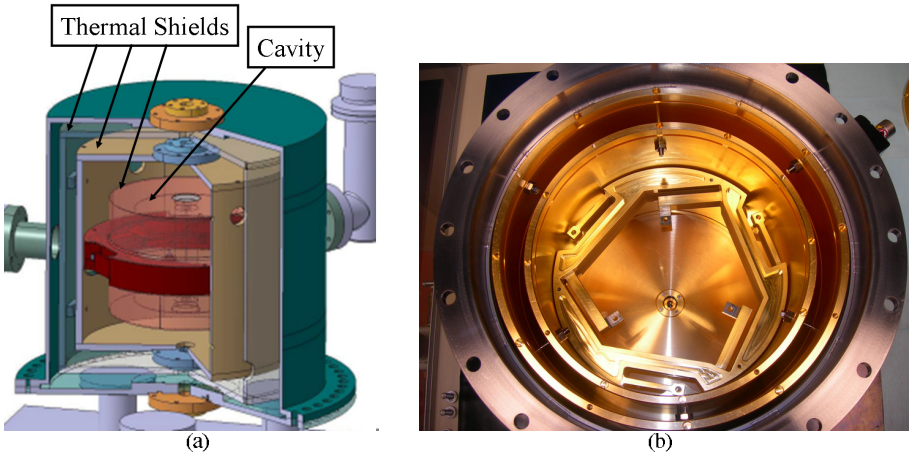

Fig. 3. (a) Drawing of the system including cavity, interface, shields and vacuum chamber. (b) Photography of the whole system except the cavity. The CFD is visible with its inner and outer cantilevers, see paragraph 2.2 for details.

days respectively. This is equivalent to an overall time constant (geometric mean) of about 1.5 days. These results are based on the assumption of 90% and 95% reflectivity for the stainless steel enclosure and the shields respectively and taking in account the thermal conductance of the titanium standoffs. A third much shorter time constant due to the thermal resistance trough the CFD and to the cavity thermal capacitance is neglected in the thermal model. A simple model based on a purely radiative thermal exchange between shields would lead to an overall time constant of $\sim$2 days (second order system).

The stainless steel vacuum chamber is a cylinder with a radius of 170 mm and a height of 300 mm. The total mass of the cavity assembly (40 kg) is dominated by the mass of this external vacuum enclosure ($\sim$ 20kg). The use of titanium for future versions is preferable since for similar thermo-mechanical properties, the density of this material is 40% lower. A 2 liter/second ion pump ensures a vacuum level $< 10^{-6}$ mbar. A residual gas analysis showed that the molecular hydrogen H_2 outgassing from the stainless steel enclosure limits the vacuum level. The use of titanium for the chamber material will avoid this problem.

3. Experimental test setup

The experimental setup to lock a laser onto the cavity uses the Pound Drever Hall (PDH) method [24]. The scheme and a picture of the setup are presented in Fig. 4. We use a low noise extended cavity laser diode (RIO Planex) with a linewidth <10kHz and an output optical power of 15mW. A fibered voltage controlled Variable Optical Attenuator (VOA) is used to control the optical power sent into the cavity. A 10/90 splitter extracts 90% of the frequency stabilized beam. A polarizing beam splitter and a half waveplate allow fine tuning of the optical power. After passing through an optical isolator, the beam is phase modulated at 61MHz using an Electro-Optical Modulator (EOM). We optimize the light polarization state before the EOM in order to minimize the residual amplitude modulation. A high modulation frequency allows a potentially large control bandwidth. Additionally, the value of the frequency is chosen to minimize the influence of the nearly-degenerated modes. We use two lenses to realize the mode-matching before injecting the beam into the cavity. The reflected beam is sensed with an avalanche photodiode. The detected signal is amplified, filtered and then mixed with a local

#172506 - $15.00 USD Received 12 Jul 2012; accepted 5 Oct 2012; published 25 Oct 2012

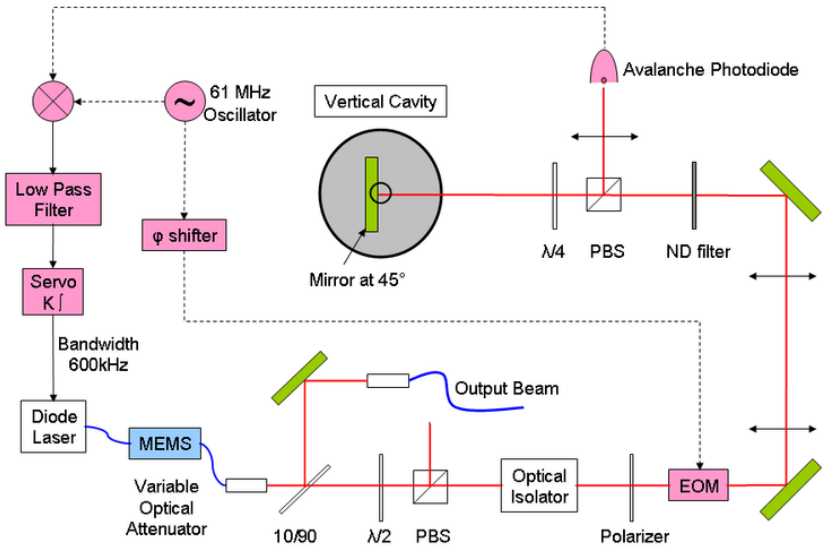

(a)

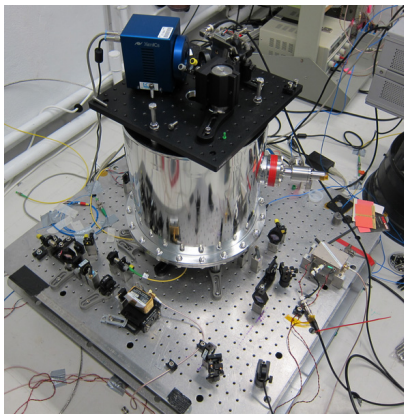

(b)

Fig. 4. (a) Experimental setup to PDH lock the laser diode. Blue line: optical fiber path, red line: free space path, black line: electrical path. PBS: Polarizing Beam Splitter, $\lambda/2(4)$: half (quarter) waveplate, EOM: Electro-Optical Modulator, ND: Neutral Density filter. (b) Photography of the experimental setup.

oscillator to produce the error signal. The control loop only acts on the injection current of the laser diode with a bandwidth of 600 kHz. This high bandwidth is obtained thanks to the use of a homemade servo electronic to drive the laser diode current instead of the commercial module (RIO Orion) that is bandwidth limited to few tens of kHz. This setup is protected against environmental perturbations by a $\sim 0.8\text{m}^3$ aluminum box with an acoustic absorber not shown in the photography of Fig. 4 and isolated from vibration by an active vibration isolation platform.

The linewidth of the cavity resonance FWHM is measured to be 3.9 ± 0.1 kHz, corresponding to a finesse of $\sim 380\,000$ (see Fig. 5(a)). The normalized reflection on resonance is < 0.2. The measurement was done by offset phase locking the laser diode to a reference ultra-stable

#172506 - $15.00 USD Received 12 Jul 2012; accepted 5 Oct 2012; published 25 Oct 2012

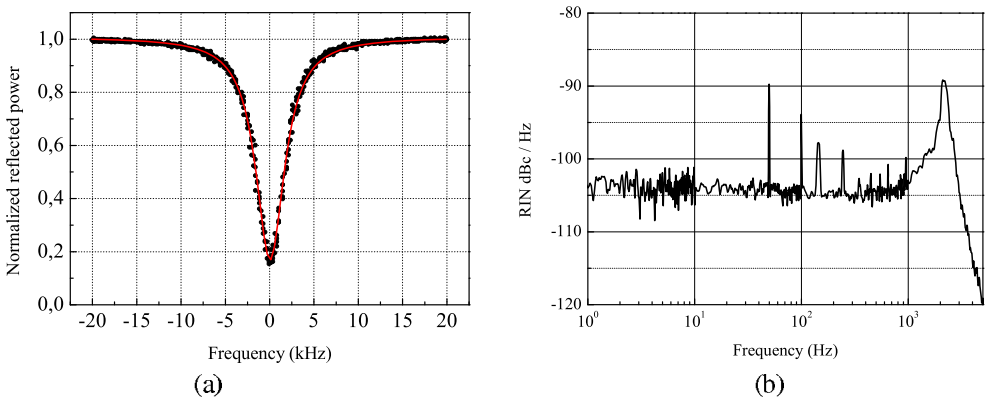

Fig. 5. (a) Plot of the normalized reflected optical power versus the laser frequency. Black squares: measured data, red curve: Lorentzian fit. (b) Out-of-loop RIN measurement of the optical power injected to the cavity.

laser (USL) [25]. This is achieved by detecting a heterodyne beat of a fraction of the laser diode output power with the USL on a fast photodiode. The RF beat-note signal is then mixed with a tunable RF synthesizer to obtain an error signal to be used for the phase locking. Frequency tuning and modulation of the RF synthesizer allow for a precise scan to be made over the resonance. We measure the optical power to frequency conversion coefficient to be about $\sim$ 200 Hertz per μWatt transmitted by the cavity. This coefficient can lead to a degradation of the frequency stability if the optical power varies with time. To avoid it, the injected optical power is actively controlled by the VOA. This system maintains a relative intensity noise (RIN) below -100 dBc/Hz from 1 Hz to $\sim$ 2kHz (Fig. 5(b)). For 4 μW of transmitted power, the frequency fluctuations induced by optical power are lower than 1×10^{-16} at 1s.

4. Characterization of the cavity assembly

4.1. Vibration sensitivity measurements

The cavity device was designed to minimize the effects of residual vibration in order to reduce frequency noise. The vibration measurement setup to evaluate its performances is presented

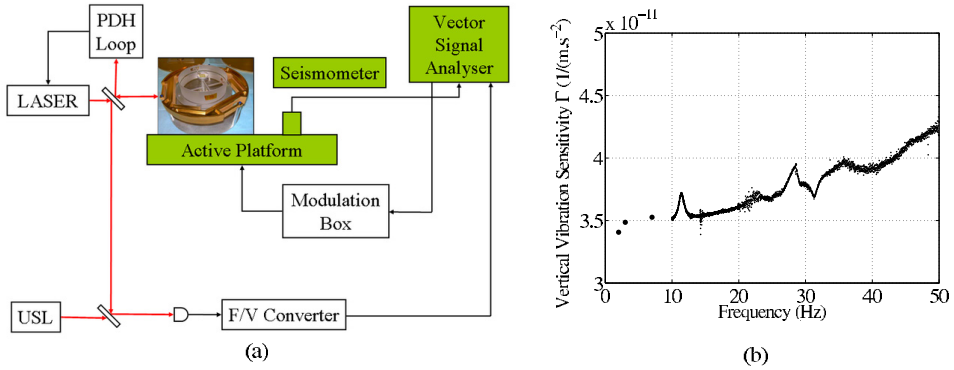

Fig. 6. (a) Vibration Sensitivity measurement setup. (b) Vertical vibration sensitivity $\Gamma(f)$ (Eq. 1) as a function of the modulation frequency.

#172506 - $15.00 USD Received 12 Jul 2012; accepted 5 Oct 2012; published 25 Oct 2012

in Fig. 6(a). The cavity setup is shaken with either sinusoidal or chirped signals from 2 to 50 Hz using an active vibration isolation platform. The upper limit of frequency is fixed by the platform. The acceleration modulation is evaluated with a piezoelectric sensor. The induced frequency modulation is measured using the beat-note between the laser diode locked to the cavity and an USL [25]. Frequency fluctuations are then converted with a homemade frequency-to-voltage (F/V) converter. Both acceleration and frequency modulations are simultaneously obtained with a vector signal analyzer. The vibration sensitivity $\Gamma(f)$ is then defined by the following equation:

$$\Gamma(f) = \frac{1}{\nu_0}\sqrt{\frac{S_\nu(f)}{S_a(f)}} \tag{1}$$

where $S_\nu(f)$ and $S_a(f)$ are respectively the frequency and acceleration power spectral densities and ν_0 is the optical frequency equal to 194 THz. With this setup, we evaluate the vertical vibration sensitivity to be $(4 \pm 0.5) \times 10^{-11}/(\mathrm{m.s}^{-2})$, see Fig. 6(b). This value is larger by one order of magnitude than the one expected from worst case FEM. We suspect that it is due to residual tensile force imbalance in the complex mechanism of washers used to bind the cavity to the CFD. Nevertheless, this preliminary result is satisfactory and encouraging considering the complexity of the system and the design constraints (rigid mounting, large temperature and acceleration range,...). The horizontal sensitivity is more difficult to evaluate due to a strong coupling between the three orthogonal axes of the platform when a horizontal excitation is applied. Nevertheless, by modulating at discrete frequencies where the cross-coupling is minimum, we can evaluate the horizontal vibration sensitivity to be $(6 \pm 3) \times 10^{-12}/(\mathrm{m.s}^{-2})$.

4.2. Thermal shielding factor evaluation

Passive thermal shielding is an efficient way to reduce the overall temperature sensitivity on short time scales. From FEM, we expect a 2^{nd} order low pass filtering with time constants of ~ 0.9 and ~ 2.5 days. To check these predictions, we apply a short temperature perturbation of $\sim 4°$C. We simultaneously record the frequency of the laser locked onto the cavity and the temperature, as shown in Fig. 7. We find that the passive thermal shielding can be modeled

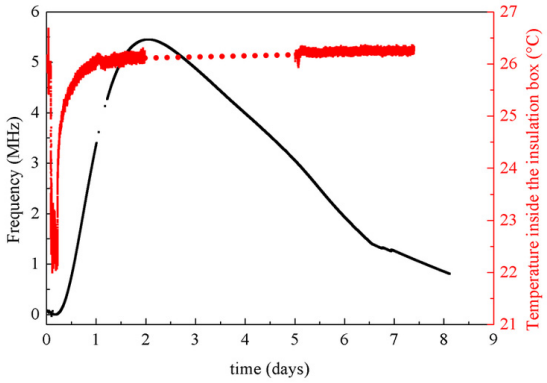

Fig. 7. Evaluation of the thermal shielding. Response of the temperature of the air surrounding the cavity vacuum enclosure (red - right scale) and the frequency of the cavity resonance (black - left scale) to a perturbation of the temperature inside the insulation box. Note: The red dots, added for clarity, correspond to an interpolation of temperature data which are not recorded.

#172506 - $15.00 USD Received 12 Jul 2012; accepted 5 Oct 2012; published 25 Oct 2012

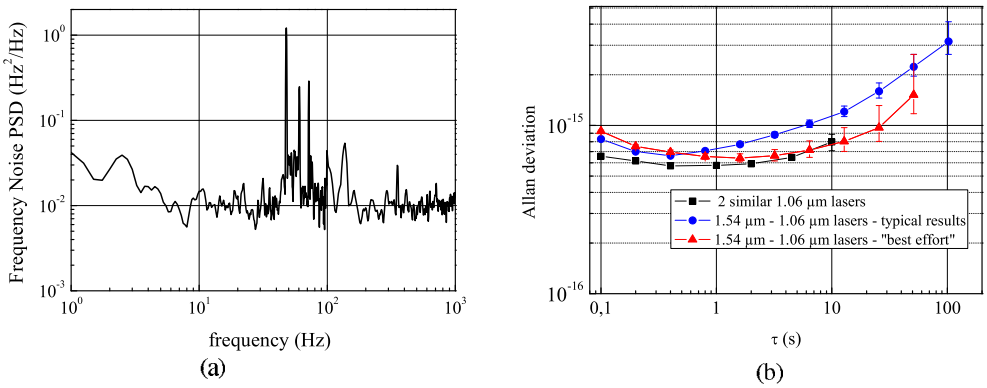

Fig. 8. (a) Frequency noise - Power Spectral Density - of the beat-note between the laser locked onto the cavity and an USL at 1.54μm. (b) Fractional frequency stability (Allan deviation) with $\pm 1\sigma$ error bars. Blue circles: Typical stability of the beat-note between one USL at 1.06μm and the laser diode lock onto the cavity at 1.54μm (2.5 Hz/s linear drift removed). Red triangle: Best results (1 Hz/s linear drift removed). Black squares: Frequency stability of the beat-note between two equivalent 1.06μm laser from reference [27].

by a second order low pass filter with a first time constant of ~ 1.3 days and a second one of ~ 2.2 days, which is equivalent to an overall time constant of ~ 1.7 days (geometric mean). This is in fair agreement with simulated values. With this thermal shielding factor, an active temperature control with a flicker noise floor of 0.1mK (Allan deviation) up to 10s is then sufficient to obtain a fractional frequency stability $< 5 \times 10^{-16}$ at 10s.

5. Frequency noise and stability

We evaluate the frequency noise of the device by measuring the beat-note with an USL. This measurement, presented on Fig. 8(a), shows a frequency noise of about 10^{-2}Hz^2/Hz from 10Hz to 1kHz. At 1Hz, the frequency noise is dominated by the USL [25]. Consequently, to evaluate the frequency stability, we use a 1.06μm laser that has been previously evaluated by comparison to a nearly identical system [26, 27]. This 1.06μm lasers beat-note frequency stability, represented in black squares on Fig. 8(b), was measured to be $\sim 6 \times 10^{-16}$ at 1s. This corresponds to a $\sim 4 \times 10^{-16}$ 1s-stability for each system under the assumption that they are identical and independent. A femtosecond fiber comb laser is then used to bridge the frequency gap between the 1.54μm and 1.06μm lasers (88THz). The contribution of the self referenced fiber comb laser is lower than $< 2 \times 10^{-16}$ from 0.1 to 10 seconds. The typical frequency stability of the 1.54μm-1.06μm beat-note is below 1×10^{-15} from 0.1 to 6 seconds (2.5 Hz/s linear drift removed) and reaches 7×10^{-16} at 1s (blue circles on Fig. 8). After 10 seconds, the stability is degraded due to a lack of active thermal control. After a long settling time, we can observe a frequency stability $< 1 \times 10^{-15}$ from 0.1 to 30 seconds after removing a linear drift of 1 Hz/s (red triangles on Fig. 8) and, after removing the contribution of the 1.06μm laser, a 1s-stability of about 5.5×10^{-16}, which is close to the expected thermal limit of 4×10^{-16}.

6. Conclusion

We report the characterization of a full industrial engineering model of FP cavity assembly for space applications. This cavity was studied, realized and assembled by SODERN space company under CNES (French Space Agency) procurement and transported to SYRTE for tests. The system was designed to be robust, transportable, and able to withstand acceleration up

#172506 - $15.00 USD Received 12 Jul 2012; accepted 5 Oct 2012; published 25 Oct 2012

to several g and temperature variations of $(20 \pm 53)^{\circ}$C. Extensive thermo-mechanical modeling was performed to reduce thermal and vibration sensitivities. The passive thermal shield acts as a second order low pass filter with an equivalent time constant being about 1.7 days, compatible with the estimated values obtained by thermal modeling. The measured axial vibration sensitivity is about 4×10^{-11}/(m.s^{-2}), while that in the transverse direction is about 6×10^{-12}/(m.s^{-2}). Although the axial coefficient is larger than that expected from the design, these values of acceleration sensitivity would be sufficient in a satellite environment with acceleration below 10^{-5}m.s$^{-2}/\sqrt{\text{Hz}}$. A laser diode locked onto the cavity shows fractional frequency stability $< 10^{-15}$ from 0.1 to few seconds and $\sim\ 5-6\ \times\ 10^{-16}$ at 1s. This stability is close to the estimated thermal limit ($\sim 4 \times 10^{-16}$). The frequency noise of the device is at a value of 10^{-2}Hz^2/Hz in the frequency range 10Hz-1kHz.

A similar device is under development for the interrogation laser of a Strontium lattice clock (698nm), in the FP7/SOC2 European project framework. Regarding the good performances of this first prototype, minor modifications of the design can lead to a significant reduction of the overall mass and the thermal sensitivity (optimization of titanium enclosure and implementation of ULE compensation ring on mirror substrates). Additionally, for applications with lower frequency stability requirements, the use of a shorter cavity (50/70 mm) will lead to a strong improvement of the main critical parameters for space applications (mass, volume, resonance frequency and acceleration tolerance).

Acknowledgments

Authors thank W. Zhang, Z. Xu and Y. Le Coq for their contribution to the frequency stability measurements and J. Pinto and M. Lours for their assistance with the electronics.

#172506 - $15.00 USD Received 12 Jul 2012; accepted 5 Oct 2012; published 25 Oct 2012